Influence of potential fluctuations on electrical transport and optical properties in modulation-doped GaN/$Al_{0.28}Ga_{0.72}N$ heterostructures

A. V. Buyanov, J. P. Bergman, J. A. Sandberg, B. E. Sernelius, P. O. Holtz, and B. Monemar
Department of Physics and Measurement Technology, Linköping University, S-581 83 Linköping, Sweden

H. Amano and I. Akasaki
Department of Electrical and Electronic Engineering, Meijo University, 1-501 Shiogamaguchi, Tempaku-ku, Nagoya 468, Japan

(Received 24 November 1997; revised manuscript received 19 February 1998)

We report transport and optical data for GaN/$Al_{0.28}Ga_{0.72}N$ modulation-doped heterostructures grown by metal-organic chemical-vapor deposition. Variable temperature galvanomagnetic, resistivity, photoluminescence, and photoconductivity measurements have been performed. Evidence for potential fluctuations is provided by the observation of weakly localized transport at low temperatures, together with a negative magnetoresistance due to disorder in the interface region. The deduced localization criteria based on the theoretical modeling from Hall, resistivity and negative magnetoresistance data are in a reasonable agreement with weak-localization conditions. Additional evidence for a built-in electric field caused by the fluctuations near the heterointerface region is given by the observation of photoconductivity dips resonant with free excitons, indicating free-exciton ionization. A theoretical modeling of the transport properties under various limiting scattering conditions is provided, and compared with the experimental data for the transport time and elastic lifetime. The potential fluctuations in the two-dimensional plane from the impurity distribution only are also modeled, and the results are consistent with the experimental indications for strong potential fluctuations. It is concluded that interface roughness, dislocations, and similar structural defects have a strong influence on the transport properties of the two-dimensional electron gas in these structures. [S0163-1829(98)06224-9]

I. INTRODUCTION

Modulation doping, i.e., doping of the barrier layer at a heterointerface, causes a redistribution of electrical charge across the interface. In the case of n-type doping of the barrier layer, the region in the barrier close to the interface will be depleted and the corresponding electrons accumulated in a triangular shape potential in the active layer close to the interface.[1] The electrons accumulated in the potential form a two-dimensional electron gas (2DEG). The properties, electrical and optical, related to the 2DEG electrons have previously been extensively studied by several groups, mainly in the GaAs/$Al_xGa_{1-x}As$ (Refs. 2–6) but also in the $In_xGa_{1-x}As$/InP material system.[7] The formation of a 2DEG at a GaN/$Al_xGa_{1-x}N$ heterointerface has previously been observed by electrical measurements,[8,9] and recently by optical spectroscopy.[10]

Since the possibilities of epitaxial growth of III-nitride structures are still limited to heteroepitaxy on sapphire or SiC substrates, it has been difficult to obtain high-quality epilayers in GaN/$Al_xGa_{1-x}N$ modulation-doped heterostructures (MDH's). Dislocations and interface roughness have strong effects on the electrical transport properties of MDH structures, amplified by the strain built in by the heteroepitaxial growth and by the related piezoelectric fields. Such defects, in addition to the "normal" scattering centers, e.g., remote ionized impurities or point defects, are the possible sources for inhomogeneities and potential fluctuations (PF's) in state of the art $Al_xGa_{1-x}N$/GaN MDH systems.

The inhomogeneities can generally be classified into two categories, depending on their characteristic size Λ with respect to the electron mean free path l. Previous studies[11,12] considered primarily the microscopic inhomogeneities with $\Lambda < l$ that originated from random fluctuations in the density of charge scattering centers, as being mainly responsible for the carrier kinetics and recombination properties for the 2DEG in MDH's. The deviation of a heterointerface from an ideal plane, i.e., the heterointerface roughness, is expected to cause strong variations in the interface potential (amplified by the built-in epitaxial strain and the piezoelectric effect), and reduce the mobility of the 2DEG localized in the direct vicinity of an interface. The potential of this type of scattering is known to be approximately proportional to the square E_b^2 of the built-in electric field E_b of the spatial fluctuation.

In the absence of a magnetic field, the electron states in a 2DEG are localized at low temperatures, due to disorder.[13,14] The corresponding fluctuations in the electrostatic potential could lead to electron localization in random potential profiles at reduced temperatures,[15] and can also provide an additional scattering process for the 2DEG free carriers.

The large-size fluctuations with $\Lambda > l$ are effectively screened by free carriers and are therefore expected to have a small effect on the carrier kinetics and recombination processes.[16]

Recent theoretical estimates of the limiting transport properties in the $Al_{0.28}Ga_{0.72}N$/GaN MDH 2DEG system indicate that the present record values (about 8000 $cm^2/V\,s$) observed at low temperatures for the mobility of the 2DEG carriers are more than two orders of magnitude below the expected limiting values (about 10^6 $cm^2/V\,s$) for corresponding $Al_xGa_{1-x}N$/GaN structures made from perfect materials.[17] The present investigations should be viewed in this perspective.

 © 1998 The American Physical Society

This work investigates experimental evidence for the presence of microscopic potential fluctuations in modulation-doped GaN/$Al_{0.28}Ga_{0.72}N$ heterostructures. We report on transport results for $Al_{0.28}Ga_{0.72}N$/GaN MDH's and compare these with predictions from weak-localization (WL) theories for a 2DEG, where spatial fluctuations and other irregularities give rise to disorder and localization. A theoretical modeling of the transport parameters as well as the potential fluctuations is also provided. The photoconductivity properties together with photoluminescence provide additional evidence for the influence of PFs on the recombination processes in this system.

II. EXPERIMENT

The investigated $Al_{0.28}Ga_{0.72}N$/GaN/AlN/sapphire MDH's were grown by metal-organic chemical-vapor deposition.[18] The GaN layer was nominally undoped (residual n doping about 1×10^{17} cm^{-3}) and 3.85 μm thick. The top $Al_{0.28}Ga_{0.72}N$ layer included a 5-nm-thick undoped spacer layer close to the GaN interface, and a 90-nm-thick layer which was Si-doped to a concentration of 3×10^{18} cm^{-3}. The transport studies were performed within the temperature range 1.5–250 K in a superconducting solenoid magnet Oxford SM 2000. Hall effect measurements were done under an applied magnetic field (B) of 0.3 T. All transport data presented in this paper were taken by a low-amplitude dc-current (1–5 μA) technique. The magnetoresistance was measured in a magnetic field up to 2 T in a direction normal to the plane of the MDH's. Measurements were made on lithographically defined Hall bars with six Al/Ti Ohmic contacts. Stationary and persistent photoconductivity measurements have been performed in a variable temperature cryostat (2–300 K) in a standard way (for details see, e.g., Ref. 19). For photoluminescence (PL) measurements, the sample was excited with a Ti:sapphire solid state picosecond pulsed tunable laser, upconverted with a BBO crystal, to obtain excitation around the GaN bandgap. The detection of the PL spectra was performed with a cooled charge-coupled device camera. Photoluminescence excitation (PLE) measurements were performed in the same setup, where the natural spectral width of the pulsed laser limited the spectral resolution to about 2 meV. Time-resolved measurements were performed with a Hamamatsu Syncroscan streak camera system.

III. EXPERIMENTAL RESULTS

In this section we describe the experimental observations and their interpretation. We start with an analysis of variable temperature resistivity and Hall-effect measurements. The corresponding data, together with the results from negative magnetoresistance, are discussed in terms of weakly localized transport, where spatial fluctuations and other irregularities give rise to disorder and localization. The data from optical characterization (PL, PLE, photoconductivity) are then discussed, and a connection is made with the transport properties caused by the presence of fluctuation potentials.

A. Electrical transport in GaN/$Al_{0.28}Ga_{0.72}N$ modulation-doped heterostructures

The variation of the total resistivity ρ_{tot} with temperature is shown in Fig. 1. There are three different temperature intervals where ρ_{tot} shows a characteristic dependence versus temperature. In the initial low-temperature range the value ρ_{tot} decreases slightly with T, demonstrating, as we show later, the weakly localized transport. The conductivity transition from this one to free carrier transport is observed at $T=10$–25 K. The ''high'' temperature interval $T>100$ K shows the well-known phonon assisted increase of ρ_{tot} with T.

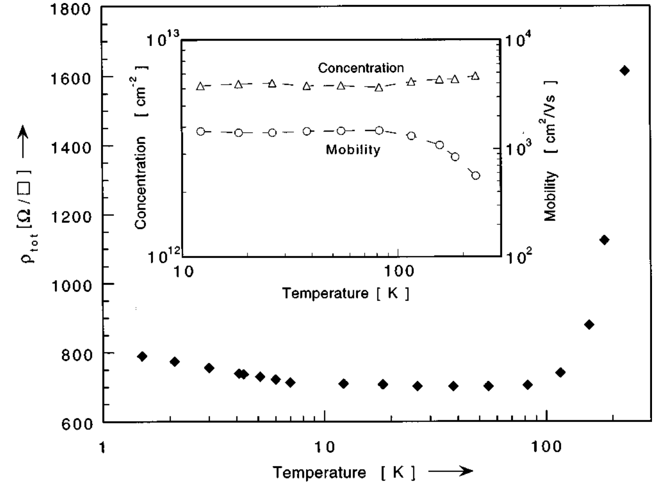

FIG. 1. Total resistivity vs temperature for the $Al_{0.28}Ga_{0.72}N$/GaN modulation-doped structure. In the inset is shown the corresponding total carrier concentration (△) and total mobility (○) vs temperature.

The inset in Fig. 1 shows the temperature dependence of mobility and sheet electron concentration in the temperature interval for free carrier transport. The total MDH electron mobility increases with decreasing temperature and saturated at a value of $\mu=1470$ $cm^2/V\,s$ at 80 K. It also remained fairly constant for temperatures between 80 and 10 K. The total sheet concentration is practically constant ($n_{sheet}\approx6.2\times10^{12}$ cm^{-2}) within the entire temperature range and clearly exhibits degenerate conduction. We attribute this behavior of the electron mobility and the metal-like or degenerate conductivity in the heterostructure to the formation of a 2DEG at the GaN-$Al_{0.28}Ga_{0.72}N$ interface, and in addition a degenerate electron channel in the $Al_{0.28}Ga_{0.72}N$ layer.

It is important to note, that the individual conductivity channels have very small B dependencies on their own, so that the measured strong B dependence arises mainly from the mixed-conductivity (parallel conduction) effect. The clearly increasing magnetoresistance and decreasing Hall coefficient values with increasing magnetic field are indicative of a significant parallel conduction in our samples (i.e., there is a conducting channel in the $Al_{0.28}Ga_{0.72}N$ barrier) within the entire temperature range, 1.5–250 K. For the proper analysis of this situation the well-known classical magnetic-field equations[20] are either numerically fitted to the data or approximated to get an analytical two-channel solution at small magnetic fields. For the data in this paper we use the exact analytical two-channel solution for the MDH system, similar to that developed by Look, Stutz, and Bozada,[21] which holds at arbitrary B as long as the carriers are degenerate and quantum effects can be ignored. This solution is much more useful than an approximate low-B solution, be-

cause high values of B give better signal to noise ratio. It is also obviously more useful than a numerical fit to the original equations,[19] because the latter requires a four-parameter fit. We found that both "transport channels" (i.e., the $Al_{0.28}Ga_{0.72}N$ doping region and the GaN 2D region, respectively) exhibit degenerate conduction within the temperature interval 30–220 K. In the case of the GaN 2D conductivity (i.e., the modulation-doped channel in the GaN layer) we estimate the mobility and sheet concentration at $T=54$ K to 2950 cm^2/V s and 1.5×10^{12} cm^{-2}, respectively. The corresponding values for the $Al_{0.28}Ga_{0.72}N$ channel at the same temperature is $\mu_{3D}=890$ cm^2/V s and $n_{3D}=4.9\times10^{12}$ cm^{-2}.

The possible existence of more than two conducting channels was carefully considered. Including a third channel gives valid solutions only for a conductivity of the third channel less than a few percent of the total conductivity. The possible third channel would be close to the highly defective GaN sapphire interface. In this case the 3.85-μm-thick GaN layer should not allow the contact metallization diffusion front to penetrate to the GaN/sapphire interface during a few minutes processing at about 600 °C. We therefore feel confident that our two-channel treatment is valid.

In comparison with the theoretical analysis by Hsu and Walukiewicz[17] for the intrinsic mobility limits of a 2DEG in $Al_{0.28}Ga_{0.72}N$/GaN heterostructures, the mobilities determined in our study are more than two orders of magnitude lower than the theoretically predicted values for the "perfect" MDH in this materials system. In the following we will argue, that an important mobility limiting mechanism in this system is scattering via fluctuation potentials in the interface region (the modulation-doped channel in the GaN layer).

A striking effect of quantum interference is to enhance the probability for backscattering in a "slightly" disordered system in the metallic (or degenerate as for the 2DEG in a MDH) regime. This effect has been interpreted as a precursor of localization in a strongly disordered systems and has thus become known as weak localization.[14] This effect predicts a logarithmic temperature dependence for $\rho(T)$ for 2D WL systems.[13] The application of a magnetic field perpendicular to the 2DEG suppresses the WL effect and the resulting negative magnetoresistance (NMR) is the most convenient way to resolve experimentally the WL correction.[22,23] This NMR-effect is based on the quantum interference of an electron with itself along a diffusion loop. The magnetic field shifts the phase of the electronic wave function and destroys the localization effect, giving rise to the NMR. Taking into account the high density of disorder and irregularities in present-day nitride-based heterostructures (due to dislocations and interface roughness amplified by built-in strain and piezoelectric fields, in addition to the "normal" scattering centers such as remote ionized impurities), it can be concluded that the experimental observation of WL transport is one convincing piece of evidence for the expected potential fluctuations in the $GaN/Al_{0.28}Ga_{0.72}N$ MDH system.

As can be seen in Fig. 2, ρ_{2D} [as distinguished from ρ_{tot} (Ref. 20)] exhibits a logarithmic temperature dependence $r\sim-\ln(T)$ in the temperature interval 1.5–10 K, typical for a weakly localized 2DEG. Additional evidence is provided by the observation of NMR in the same temperature range, as shown in the inset of Fig. 2. The deduced localization criteria $k_F l=8.6$ (k_F is the electron Fermi wave vector; l the electron

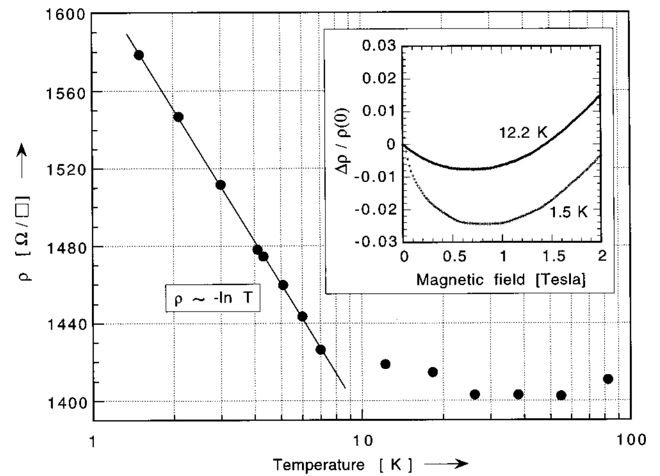

FIG. 2. An exponential fit of the resistivity of the 2DEG at the $Al_{0.28}Ga_{0.72}N$/GaN interface vs temperature in the low-temperature region. The inset shows the negative magnetoresistance data, at two different temperatures.

mean free path) from Hall, resistivity and NMR data are in an agreement with the transport criteria under weak-localization conditions, $k_F l\gg1$.[14]

B. Optical characterization and photoconductivity

The optical experiments provide additional evidence for the presence of potential fluctuations in the $GaN/Al_{0.28}Ga_{0.72}N$ MDH samples, because the built-in electric field from these fluctuations modifies the carrier recombination and nonequilibrium transport under photoexcitation.

The most striking experimental result is the observation of exciton ionization by the built-in electric field from PF's. We show in Fig. 3 a set of PL spectra at different temperatures for the modulation-doped $GaN/Al_{0.28}Ga_{0.72}N$ heterostructure. The 2-K spectrum is dominated by the donor bound exciton (DBE) at 3.490 eV, originating from the compressively strained GaN layer close to the 2DEG (the excitation depth

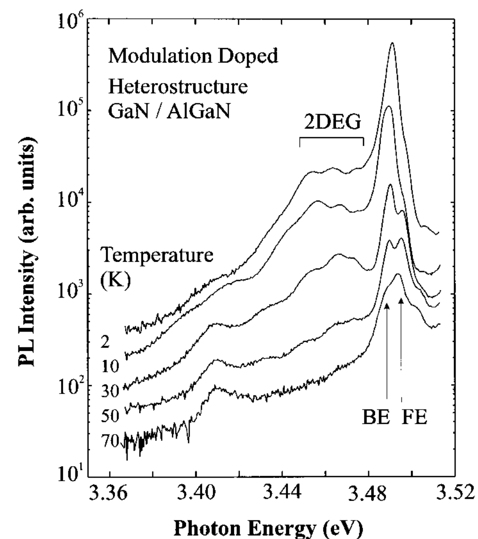

FIG. 3. Photoluminescence spectra at various low temperatures, obtained with excitation above the GaN band gap.

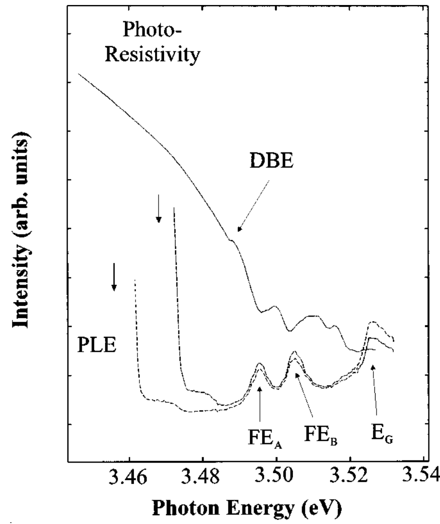

FIG. 4. PLE spectra at 2 K for the $Al_{0.28}Ga_{0.72}N/GaN$ structure, obtained with detection at two different photon energies (indicated by arrows). The photoresistivity spectrum of the same sample is also shown ($T=2$ K).

goes considerably beyond the extension of the 2DEG). At higher temperatures, when the DBE is thermally quenched, the *A* and *B* states of the free exciton (FE) are also observed, at slightly higher energies. The weaker emission at 3.41 eV is the LO-phonon replica of the free exciton. The remaining broad emission band in the energy range between 3.44 and 3.48 eV is attributed to recombination processes related to electrons in the 2DEG. The 2DEG related emission in our sample has a time decay ranging between 200 and 250 ps, with a longer decay towards the low-energy side. This causes a small redshift of the emission with increasing time delay after the pulsed excitation, which is typical for emissions related to the 2DEG in corresponding $GaAs/Al_xGa_{1-x}As$ structures.[5,6] The decay times of the FE and the DBE was measured to 50 and 80 ps, respectively. The rather low values of these decay times[24] indicate that they are all dominated by a nonradiative shunt path [i.e., capture (transfer) of excitons to defects] under these (low-intensity) excitation conditions.

PLE measurements have also been performed on this sample, and are shown in Fig. 4. With detection at two energy positions in the 2DEG related emission, as indicated with arrows in the figure, we observe two distinct excitation resonance's at higher energies. We attribute this to the resonant excitation of the *A* and *B* state of the FE in the GaN layer closest to the 2DEG. The same state is also observed during detection in the DBE. We see no feature related to states in the interface notch or to the Fermi edge. From this we conclude that the main generation mechanism for the 2DEG emission is by optical excitation of free carriers and FE's in the flat band part of the GaN layer, which afterwards diffuse to the interface region. This is confirmed by the time-resolved measurements, where a longer lifetime and delay of the intensity is seen for the 2DEG emission, as compared to the temporal behavior of the DBE and FE emissions.

The photoresistivity, between two surface contacts, versus excitation energy is shown in Fig. 4, together with the PLE measurements. As for the PLE we observe resistivity dips,

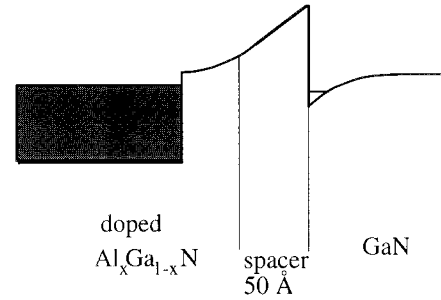

FIG. 5. Schematic profile of the modulation-doped $Al_{0.28}Ga_{0.72}N/GaN$ structure, used in the theoretical modeling. To the left is shown the degenerate (3D) $Al_{0.28}Ga_{0.72}N$ channel, while the 2DEG is confined to a narrow region at the $Al_{0.28}Ga_{0.72}N/GaN$ interface.

corresponding to an increased conductivity, resonant with the FE *A* and *B* states. Since excitons by themselves are not causing conductivity there must be a mechanism present that produces free carriers. The mechanism suggested here is that the FE is ionized by the built-in electric field in the interface region. This mechanism (presumably dominated by impact ionization) will produce free carriers, which explains both the decrease in resistivity and the increased intensity of the 2DEG related emission.

IV. THEORETICAL MODELING OF TRANSPORT IN THE $Al_{0.28}Ga_{0.72}N/GaN$ MDH SYSTEM

A schematic energy diagram for the sample is shown in Fig. 5. The $Al_xGa_{1-x}N$ side is heavily *n*-type doped with approximately 3×10^{18} cm^{-3} donor density, except for a 50-Å-wide undoped spacer region near the GaN interface.

Electrons have been transferred from the heavily doped region to the triangular well formed on the GaN side of the interface. The 2D electron density in this well is experimentally found to be 1.5×10^{12} cm^{-2}, which means that a 50-Å-wide depletion region has been formed. Thus ideally the system consists of a 3D metallic region, a 50-Å-wide depletion region with randomly distributed Coulomb potentials from the ionized donors, a 50-Å-wide spacer layer followed by a quasi-2D electron gas. We neglect the width of the 2D gas. Also we neglect the piezoelectric fields in this modeling. The electron contribution from the GaN layer is comparatively small (residual donor doping in GaN about 10^{17} cm^{-3}), and is also neglected here for simplicity.

The presence of the 3D metallic region to the left of the scattering centers (Fig. 5) should contribute to the screening of the impurities. For a perfectly conducting metal the result would be a mirror charge for each impurity. Now, the region is not a perfect metal. The Thomas-Fermi screening length is 21 Å for our particular carrier density. Impurities much farther away from the surface of the 3D metallic region than this distance will produce mirror charges, while the impurities closer to the surface will be screened to a lesser extent. We have made two extreme transport calculations where in one case the screening from the 3D region was completely neglected, and in the other case all scatterers as well as all induced charge distributions in the 2D layer give rise to mirror charges in the 3D surface. In a third calculation we have

neglected the influence from the 3D region and also put all the impurities in the 2D layer. We have calculated the transport time and elastic lifetime with these three different assumptions and compared them to the experimentally extracted values.

In the modelling we need the static 2D dielectric function. It is in random phase approximation given by[25]

$$\varepsilon(Q)=1-\nu_Q\chi_0(Q)$$
$$=\{1+y/Q;Q<1,1+y/Q\{1-\sqrt{1-1/Q^2}\};Q>1\}. \tag{1}$$

We have here introduced the density parameter y and the renormalized momentum Q. These and other dimensionless variables used throughout are defined as

$$W=\hbar\omega/4E_F,\quad E_F=\hbar^2k_F{}^2/2m^*,$$
$$Q=q/2k_F,\quad y=m^*e^2/\hbar^2\kappa k_F,$$
$$D=d\cdot 2k_F,\quad D_0=d_0\cdot 2k_F. \tag{2}$$

We have in our calculations used the values 0.21 for the electron mass and 9.9 for the dielectric constant for GaN.

The experimentally obtained values were for the transport time, estimated from the low-temperature conductivity, and for the elastic lifetime, estimated from the magnetic-field variation of the conductivity. This last estimate relies on the assumption that the low-temperature results follow weak-localization theory.

A. Extraction of transport data from experimental results

The 2DEG resistivity was estimated to be 1410 Ω/□ at 54 T. The transport time for the carriers in the 2DEG was obtained from the Drude-type relation

$$1/\rho=\sigma=ne^2\tau_{\mathrm{tr}}/m^*=ne\mu\Rightarrow\tau_{\mathrm{tr}}=m^*\mu/e. \tag{3}$$

This gives a value of 0.352 ps for the transport time τ_{tr}.

A value for the elastic lifetime was estimated from the magnetic-field variation of the conductivity. Again, this estimate relies on the assumption that the low-temperature results follow weak-localization (WL) theory.

From studying the magnetic-field dependence of the conductivity we may extract values for the dephasing time and elastic lifetime. According to the weak-localization theory the magnetic conductivity corrections are given by[22,23]

$$\Delta\sigma_{\mathrm{WL}}^{\mathrm{2D}}(B_\perp)\equiv\sigma_{\mathrm{WL}}^{\mathrm{2D}}(B_\perp)-\sigma_{\mathrm{WL}}^{\mathrm{2D}}(0)$$
$$=\frac{e^2}{2\pi^2\hbar}\left[\psi\left(\frac{1}{2}+\frac{B_{ph}}{B_\perp}\right)-\psi\left(\frac{1}{2}+\frac{B_e}{B_\perp}\right)+\ln\left(\frac{B_e}{B_{ph}}\right)\right], \tag{4}$$

where ψ is the digamma function, $\psi(x)=(d/dx)\Gamma(x)$, and

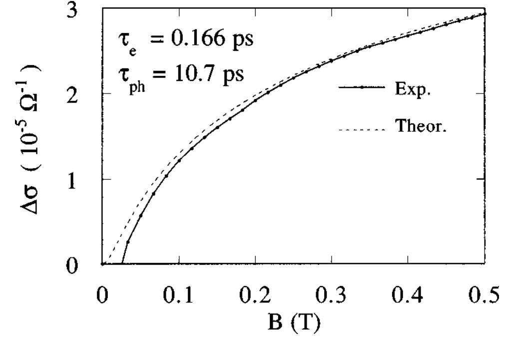

FIG. 6. A fit of the experimental data for magnetoconductivity to Eq. (4). The extracted values for τ_e and τ_{ph} are also shown.

$$B_{ph}=\frac{\hbar}{4eD\tau_{ph}},$$
$$B_e=\frac{\hbar}{4eD\tau_e}, \tag{5}$$

where D is the diffusivity or diffusion constant, $D=1/2\,v_F^2\tau_e$, and τ_e (τ_{ph}) is the elastic lifetime (dephasing time). The unknown variables are the two characteristic scattering times. These are extracted from a fit to the experimental results. The fit is shown in Fig. 6.

The extracted values from the fit are

$$\tau_e=0.166\ \ \mathrm{ps},$$
$$\tau_{ph}=10.7\ \ \mathrm{ps}.$$

B. Transport modeling

In this section we calculate the transport time and elastic lifetime for the ideal system. The transport time is derived with the generalized Drude approach.[26] The elastic lifetime is obtained from the imaginary part of the electron self-energy at the Fermi level. The self-energy is obtained with the Rayleigh-Schrödinger perturbation theory[27] from the electron-impurity interaction energy to second order in the potential.

1. All scatterers in the 2D layer

Putting all impurities in the 2D layer leads to an extreme overestimation of the impurity scattering since it completely wipes out the intended benefit from spatially separating the carriers and scattering centers. The transport time can be found from the simple integral[28]

$$1/\tau_{\mathrm{tr}}=\frac{2m^*e^4}{\hbar^3\kappa^2}\int_0^1\frac{dQ}{\varepsilon(Q)^2\sqrt{1-Q^2}}, \tag{6}$$

and the numerical result is $\tau_{\mathrm{tr}}=0.0326$ ps.

The elastic lifetime is obtained from the imaginary part of the self-energy for an electron at the Fermi surface. This is

$$\mathrm{Im}\,\Sigma=-\frac{m^*e^4}{2\hbar^2\kappa^2}\int_0^1\frac{dQ}{\varepsilon(Q)^2Q^2\sqrt{1-Q^2}}=\begin{cases}-\frac{yE_F}{y^2-1}\left[\frac{2y^2}{\sqrt{y^2-1}}\tan^{-1}\sqrt{\frac{y-1}{y+1}}-1\right], & y>1,\\ -\frac{2E_F}{3}, & y=1,\\ -\frac{yE_F}{y^2-1}\left[\frac{y^2}{\sqrt{1-y^2}}\ln\left(\frac{1+y+\sqrt{1-y^2}}{1+y-\sqrt{1-y^2}}\right)-1\right], & y<1.\end{cases} \quad (7)$$

Thus it is possible to solve the equation and find the result in an analytical form. Now, the lifetime is

$$\tau_e=-\frac{\hbar}{2\,\mathrm{Im}\,\Sigma}. \quad (8)$$

The numerical result for the elastic lifetime is 0.0248 ps. Both of these theoretically obtained times are much too short, which is what we had anticipated (see Table I).

2. Scatterers randomly distributed in the region between the 3D layer and the spacer with screening from the 3D layer neglected

Let d be the distance between the 3D and 2D regions and d_0 the thickness of the spacer layer. As compared with the strictly 2D treatment [Eqs. (6) and (7)] the integrands will have the additional factor

$$\frac{1}{D-D_0}\int_{D_0}^{D}e^{-2QZ}dZ=\frac{e^{-Q(D+D_0)}}{Q(D-D_0)}\sinh[Q(D-D_0)]. \quad (9)$$

Thus we have

$$1/\tau_{\mathrm{tr}}=\frac{2m^*e^4}{\hbar^3\kappa^2}\int_0^1\frac{e^{-Q(D+D_0)}\sinh[Q(D-D_0)]}{\varepsilon(Q)^2Q(D-D_0)\sqrt{1-Q^2}}\,dQ, \quad (10)$$

and the numerical result is now $\tau_{\mathrm{tr}}=4.18$ ps for the transport time.

For the elastic lifetime we have

$$\mathrm{Im}\,\Sigma=-\frac{m^*e^4}{2\hbar^2\kappa^2}\int_0^1\frac{e^{-Q(D+D_0)}\sinh[Q(D-D_0)]}{\varepsilon(Q)^2Q^3(D-D_0)\sqrt{1-Q^2}}\,dQ \quad (11)$$

and the numerical result for the elastic lifetime τ_e is 0.197 ps. Both these times (τ_{tr} and τ_e) are too long compared to the experimental values.

TABLE I. Results from calculations of transport time and lifetime.

	Transport time (ps)	Elastic lifetime (ps)
Experiment	0.352	0.166
Impurities in 2D layer	0.0326	0.0248
No image potential	4.18	0.197
Full image potential	8.20	1.01

3. Scatterers randomly distributed in the region between the 3D layer and spacer, full image-potential screening from the 3D layer

In this case the potentials have to be determined self-consistently. We have

$$\nu=\nu_qe^{-qz}-\nu_qe^{-q(d+d-z)}+\rho_{\mathrm{ind}}\nu_q-\rho_{\mathrm{ind}}\nu_qe^{-q2d},$$

$$\rho_{\mathrm{ind}}=\chi_0\nu, \quad (12)$$

where ν is the potential in the 2D plane from a Coulomb potential a distance z from the plane. The potential ν_q is the bare Coulomb potential, only screened by the background dielectric constant, and ρ_{ind} and χ_0 are the induced charge density in the 2D layer and the susceptibility of the 2D layer, respectively.

Solution of these coupled equations gives

$$\nu=\frac{\nu_qe^{-qd}2\sinh[q(d-z)]}{1-\chi_0\nu_q(1-e^{-q2d})}. \quad (13)$$

As compared with the strictly 2D treatment the screening will be modified and the integrands will have the additional factor

$$2e^{-2QD}\left(\frac{\sinh[2Q(D-D_0)]}{2Q(D-D_0)}-1\right). \quad (14)$$

Thus we have

$$1/\tau_{\mathrm{tr}}=\frac{2m^*e^4}{\hbar^3\kappa^2}\times\int_0^1\frac{e^{-2QD}\{\sinh[2Q(D-D_0)]-2Q(D-D_0)\}}{\left[1+\frac{y}{Q}\,(1-e^{-2QD})\right]^2Q(D-D_0)\sqrt{1-Q^2}}\,dQ \quad (15)$$

and the numerical result is $\tau_{\mathrm{tr}}=8.20$ ps.

The imaginary part of the self-energy is

$$\mathrm{Im}\,\Sigma=-\frac{m^*e^4}{2\hbar^2\kappa^2}\times\int_0^1\frac{e^{-2QD}\{\sinh[2Q(D-D_0)]-2Q(D-D_0)\}}{\left[1+\frac{y}{Q}(1-e^{-2QD})\right]^2(D-D_0)Q^3\sqrt{1-Q^2}}dQ, \quad (16)$$

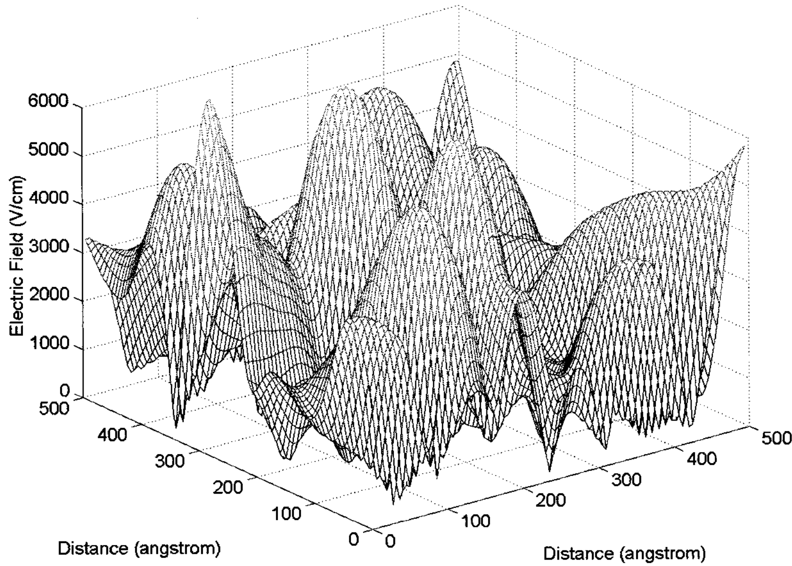

FIG. 7. Potential fluctuations over an area 500×500 Å, obtained from a simulation considering ionized impurities alone.

which leads to a numerical result for the elastic lifetime τ_e of 1.01 ps.

The results from the calculations of the transport time and lifetime with the various assumptions are summarized in Table I, together with the experimental results.

C. Modeling of the potential in the 2DEG plane

For several reasons there is an interest to find an estimate of the potential fluctuations and electric-field strengths in the plane of the 2DEG, the weak localization behavior of the low-temperature conductivity originates from the presence of potential fluctuations; the photoresistivity experiments indicate the presence of strong electric fields ionizing the excitons.

We have studied the potential in the 2D layer from the ionized impurities. Two versions were treated, one without image potentials and one with full image potentials. We chose a big square unit cell so that 1000 scatterers on the average would be within the cell. The size was 2500×2500 Å for a scatterer density of 1.6×10^{12} cm^{-2}. We modified this density slightly to get nice numbers. The ions were then distributed at random below this square and at random depth within the layer between the spacer and the 3D region; This was done with help of a random-number generator. The whole plane was then filled with equal unit cells, i.e., periodic boundary conditions were assumed. The potential from all ions was then periodic with the unit cell as period. We may say that we have constructed a crystal with a unit cell with a huge basis consisting of 1000 ions. We then studied the potential within a square in the middle of the unit cell. The square had to be small as compared to the unit cell so that we avoided surface effects. We chose a square that on the average contained 40 ions. This means a square of size 500×500 Å. The number of ions in this square varied from run to run since 1000 ions were distributed at random within the large unit cell. The potential was found as follows:

$$W(\mathbf{r})=\frac{1}{\Omega_{\substack{\text{unit}\\\text{cell}}}}\sum_{G} e^{i\mathbf{G}\cdot\mathbf{r}}\sum_{i=\text{basis}}\omega_0^i(\mathbf{G}),$$

$$G_{x,y}=\pm n\,\frac{2\pi}{L},\quad n=1,2,3\dots\ . \tag{17}$$

When the image potentials were neglected we obtained

$$\omega_0^i(\mathbf{G})=\frac{\nu_{\mathbf{G}}e^{-GZ_i}}{1-\nu_{\mathbf{G}}\chi_0(G)}\,e^{-i\mathbf{G}\cdot\mathbf{R}_i}, \tag{18}$$

and when full image potentials were included,

$$\omega_0^i(\mathbf{G})=\frac{\nu_{\mathbf{G}}e^{-GD}2\sinh[G(D-Z_i)]}{1-\nu_{\mathbf{G}}\chi_0(G)(1-e^{-2GD})}\,e^{-i\mathbf{G}\cdot\mathbf{R}_i}. \tag{19}$$

In this calculation we needed the static dielectric function also for larger momenta [see Eq. (1) above].

We considered it to be enough to include reciprocal lattice vectors up to $n=50$. For this value the exponentially decaying factor for the ion closest to the 2D layer is 1.8×10^{-3}. The potential fluctuates a little bit more when image potentials are neglected, but there is no big difference. The average built-in electric field is around 3 kVcm^{-1} and the maximum value is around 7–12 kV cm^{-1}, as presented in Fig. 7.

V. DISCUSSION

Our experimental data presented in this work are for state of the art GaN/$Al_{0.28}Ga_{0.72}N$ heterostructures grown on sapphire. The values for the mobilities in these structures are smaller than the best values recently reported,[29] but we believe this is not a significant factor in determining the physical processes that govern the transport in these structures. The effects described in this work are believed to be inherent to the state of the art GaN/$Al_xGa_{1-x}N$ modulation-doped heterostructures, grown on sapphire, and thus affected by a very large number of crystal defects (typically 10^{10} cm^{-2} dislocations threading through the 2D layer, and in addition inter-

face roughness induced by the large heteroepitaxial strain during growth).

Experimentally we find that there are two parallel conduction channels for electrons. This possibility has typically been neglected in recent literature,[30] but this parallel conduction strongly affects the analysis of data, and this fact needs to be considered in the future design of these structures. There is solid evidence for weak localization of the electrons in the 2DEG from the transport and magnetotransport data. The optical data support the idea that there are strong potential fluctuations in the 2D layer, causing a fluctuating electric field that is well above what is needed to impact ionize the excitons.[31,32]

In the theoretical modeling of the transport time, inelastic lifetime and fluctuating potential in the 2D layer, we have only considered the contribution from the ionized donors. The spacer layer is there to spatially separate the 2D carriers from the impurity potentials and thereby reduce the scattering and enhance the mobility. This means that in a system like this unintentional defects closer to the 2D layer, like unintentional dopants and interface roughness, have larger effects on the properties we have modeled than in systems without spacer layers. We made only an extreme model calculation where we placed all ionized donors in the 2D layer, to find the results one would have without spatial separation between carriers and scattering centers. The result from this calculation can serve as the extreme lower limit for the experimental transport and lifetimes. In the other two model calculations we neglected the screening effects from the 3D layer in one of them, and slightly overestimated the screening in the other. A more exact treatment would produce results somewhere in between the numbers from the two calculations. These values should be an upper limit for the experimental results, since the unintentional scattering effects are not included. This is consistent with our findings. One should also notice that the screening effects are more important for the lifetime than for the transport time. This is because the lifetime is relatively more affected by scattering processes with small momentum transfer than is the transport time, where phase space limitations suppress these processes.

The screening predominantly reduces the matrix elements for such scattering processes. To get some information about the neglected scattering centers we made a test calculation where we assumed that there is, apart from intentional doping impurities, a distribution of Coulomb potentials homogeneously throughout the sample to the right of the 3D region; these could, e.g., be due to self-compensation. We estimated how large the concentration of these needs to be to fit the experimental value for the transport time. We found the values 3.8×10^{17} and 8.7×10^{17} cm^{-3} with screening and without, respectively. These values seem to be somewhat too large for an unintentional doping concentration. The discrepancies are probably due to imperfections at the interface, not considered here.

The obtained potential fluctuations and electric field strengths should be considered as the lower limits of the real values, since only part of the scattering centers are taken into account. Still, we think the values are large enough to explain the experimental observations. The development of growth processes for this materials system will certainly take some time, but will hopefully in the future provide material with transport properties close to the ideal limit projected in Ref. 17. A modeling of the influence of the dislocations and interface roughness on the transport was not attempted in this work. We conclude, however, that these contributions are important in the samples studied. A realistic modeling of these effects needs consideration of the piezoelectric effects as well, in moderating the strain-induced potential fluctuations.[33]

VI. CONCLUSIONS

We have both experimentally and theoretically studied the transport and optical properties related to the disorder and irregularities in GaN/$Al_{0.28}Ga_{0.72}N$ modulation-doped heterostructures. The data are understandable in the context of potential fluctuations in the direct vicinity at heterointerface region. The low-temperature transport data demonstrate weak-localization behavior, and the photoconductivity measurements indicate the presence of potential fluctuations in the interface region.

The ionized donors alone do not explain the observed rather low mobilities and long elastic scattering and transport times. Interface roughness, dislocations, and piezoelectric effects associated with the GaN/$Al_xGa_{1-x}N$ interface are believed to be good candidates for the additional scattering processes needed for a quantitative explanation of the experimental transport data.

[1] G. Bastard, *Wave Mechanics Applied to Semiconductor Heterostructures* (Les Editions de Physique, Paris, 1992).

[2] R. Dingle, H. L. Stormer, A. C. Gossard, and W. Wiegmann, Appl. Phys. Lett. **33**, 665 (1978).

[3] Y. R. Yuan, M. A. A. Pudensi, C. A. Vawter, and J. L. Merz, J. Appl. Phys. **58**, 397 (1985).

[4] I. V. Kukushkin, K. V. Klitzing, and K. Ploog, Phys. Rev. B **37**, 8509 (1988).

[5] Q. X. Zhao, J. P. Bergman, P. O. Holtz, B. Monemar, C. Hallin, M. Sundaram, J. L. Merz, and A. C. Gossard, Semicond. Sci. Technol. **5**, 884 (1990).

[6] J. P. Bergman, Q. X. Zhao, P. O. Holtz, B. Monemar, M. Sundaram, J. L. Merz, and A. C. Gossard, Phys. Rev. B **43**, 4771 (1991).

[7] Q. X. Zhao, P. O. Holtz, B. Monemar, T. Lundström, J. Wallin, and G. Landgren, Phys. Rev. B **48**, 11 890 (1993).

[8] M. A. Kahn, J. M. van Hove, J. N. Kuznia, and D. T. Olson, Appl. Phys. Lett. **58**, 2408 (1991).

[9] M. A. Kahn, J. N. Kuznia, J. M. van Hove, N. Pan, and J. Carter, Appl. Phys. Lett. **60**, 3027 (1992).

[10] J. P. Bergman, T. Lundström, B. Monemar, H. Amano, and I. Akasaki, Appl. Phys. Lett. **69**, 3456 (1996).

[11] A. M. Kreshchuk, S. V. Novikov, and I. G. Savel'ev, Fiz. Tekh. Poluprovdn. **26**, 1375 (1992) [Sov. Phys. Semicond. **26**, 771 (1992)].

[12] A. M. Kreshchuk, S. V. Novikov, T. A. Polyanskaya, I. G. Savel'ev, and A. Ya. Shik, J. Cryst. Growth **146**, 153 (1995).
[13] E. Abrahams, P. W. Anderson, D. C. Licciardello, and T. V. Ramakrishnan, Phys. Rev. Lett. **42**, 673 (1979).
[14] W. J. Beenakker and H. van Houten, in *Solid State Physics, Advances in Research and Applications* (Academic, San Diego, 1991), Vol. 44.
[15] W. Walukiewicz, L. Wang, L. M. Pawlowicz, J. Lagowski, and H. C. Gatos, J. Appl. Phys. **59**, 3144 (1986).
[16] W. Walukiewicz, P. F. Hopkins, M. Sundaram, and A. C. Gossard, Phys. Rev. B **44**, 10 909 (1991).
[17] L. Hsu and W. Walukiewicz, Phys. Rev. B **56**, 1520 (1997).
[18] H. Amano, N. Sawaki, I. Akasaki, and Y. Toyoda, Appl. Phys. Lett. **48**, 353 (1986).
[19] C. H. Qiu, W. Melton, M. W. Leksono, J. I. Pankove, B. P. Keller, and S. P. DenBaars, Appl. Phys. Lett. **69**, 1282 (1996).
[20] R. L. Peritz, Phys. Rev. **110**, 1254 (1958).
[21] D. C. Look, C. E. Stutz, and C. A. Bozada, J. Appl. Phys. **74**, 311 (1993).
[22] P. M. Mensz and R. G. Wheeler, Phys. Rev. B **35**, 2844 (1987).
[23] W. Szott, C. Jedrzekjek, and W. P. Kirk, Phys. Rev. B **48**, 8963 (1993).
[24] J. P. Bergman, B. Monemar, H. Amano, I. Akasaki, K. Hiramatsu, N. Sawaki, and T. Detchprohm, in *Silicon Carbide and Related Materials 1995*, *Proceedings of the Sixth International Conference, Kyoto, Japan, 1995*, edited by S. Nakashima, H. Matsunami, S. Yoshida, and H. Harima, IOP Conf. Proc. No. 142 (Institute of Physics, Bristol, 1996), p. 931.
[25] F. Stern, Phys. Rev. Lett. **18**, 546 (1967).
[26] Bo. E. Sernelius, Phys. Rev. B **40**, 12 438 (1989).
[27] See, e.g., G. D. Mahan, *Many Particle Physics* (New York, Plenum, 1990).
[28] Bo. E. Sernelius and E. Söderström, J. Phys.: Condens. Matter **3**, 1493 (1991).
[29] J. M. Redwing, M. A. Tischler, J. S. Flynn, S. Elhamri, M. Ahouija, R. S. Newrock, and W. C. Mitchel, Appl. Phys. Lett. **69**, 963 (1996).
[30] S. N. Mohammad, A. A. Salvador, and H. Morkoc, Proc. IEEE **83**, 1306 (1995).
[31] D. Volm, K. Oettinger, T. Streibl, D. Kovalev, M. Ben-Chorin, J. Diener, B. K. Meyer, J. Majewski, L. Eckey, A. Hoffmann, H. Amano, I. Akasaki, K. Hiramatsu, and T. Detchprohm, Phys. Rev. B **53**, 16 543 (1996).
[32] F. Binet, J. Y. Duboz, E. Rosencher, F. Scholz, and V. Härle, Phys. Rev. B **54**, 8116 (1996).
[33] T. Takeuchi, S. Sota, M. Katsuragawa, M. Komori, H. Takeuchi, H. Amano, and I. Akasaki, Jpn. J. Appl. Phys., Part 2 **36**, L382 (1997).